

# A new Caputo time fractional model for heat transfer enhancement of water based graphene nanofluid: An application to solar energy

Sidra Aman<sup>b</sup>, Ilyas Khan<sup>a,\*</sup>, Zulhibri Ismail<sup>b</sup>, Mohd Zuki Salleh<sup>b</sup>, I. Tlili<sup>c</sup>

<sup>a</sup> Faculty of Mathematics and Statistics, Ton Duc Thang University, Ho Chi Minh City, Viet Nam

<sup>b</sup> Applied and Industrial Mathematics Research Group, Faculty of Industrial Sciences & Technology, Universiti Malaysia Pahang, 26300 Kuantan, Pahang, Malaysia

<sup>c</sup> Energy and Thermal Systems Laboratory, National Engineering School of Monastir, Street Ibn El Jazzar, 5019 Monastir, Tunisia

## ARTICLE INFO

### Keywords:

Graphene nanoparticles  
Caputo time fractional model  
Poiseuille flow  
Heat and mass transfer  
Nusselt number  
Solar energy  
Exact solution

## ABSTRACT

In this article the idea of Caputo time fractional derivatives is applied to MHD mixed convection Poiseuille flow of nanofluids with graphene nanoparticles in a vertical channel. The applications of nanofluids in solar energy are argued for various solar thermal systems. It is argued in the article that using nanofluids is an alternate source to produce solar energy in thermal engineering and solar energy devices in industries. The problem is modelled in terms of PDE's with initial and boundary conditions and solved analytically via Laplace transform method. The obtained solutions for velocity, temperature and concentration are expressed in terms of Wright's function. These solutions are significantly controlled by the variations of parameters including thermal Grashof number, Solutal Grashof number and nanoparticles volume fraction. Expressions for skin-friction, Nusselt and Sherwood numbers are also determined on left and right walls of the vertical channel with important numerical results in tabular form. It is found that rate of heat transfer increases with increasing nanoparticles volume fraction and Caputo time fractional parameters.

## Introduction

Mixed convection flow in a channel has gained much attention such as in thermal and nuclear power engineering. Mixed convection together with pulsatile Poiseuille flow (PPF) or simply mixed convection PPF is of great importance. In channel flow mixed convection arises due to cooling/ heating the walls of the channel. Makinde and Mhone [1] analyzed mixed convection flow with combined effect of a transverse magnetic field and radiative heat transfer of optically thin fluid passing through a channel filled with saturated porous medium and with heated bounding walls. Salem et al. [2] depicted the influence of moving lid direction on MHD mixed convection in a linearly heated cavity. They concluded that in case of mixed convection, the direction of lid is more effective than in case of forced convection. Salleh et al. [3] studied numerically mixed convection flow of a solid sphere. Aaiza et al. [4] studied mixed convection flow of nanofluid for different shapes of nanoparticles in a channel. They found that Grashof number leads to an increase in buoyancy force and hence fluid flow increases. Some other fascinating references related to this area are [5–8] and the references therein.

Scientists have made several attempts to improve the heat transfer efficiency of the conventional base fluids since these fluids have poor

heat transfer capability. Solids have higher thermal conductivities than those of fluids thus, various slurries have been produced by suspending solid particles in base fluids. Maxwell [9] introduced the idea of nanofluids for the enhancement of thermal conductivity. Choi [10] proposed experimentally the enhancement of heat transfer rate by using nano-sized particles. A vast range of research has been done on dispersing nanoparticles in base fluids [11]. Turkyilmazoglu and Pop [12] investigated closed form solutions for heat and mass transfer of natural convection for free convection flow of nanofluid containing  $Cu$ ,  $Ag$ ,  $CuO$ ,  $Al_2O_3$  and  $TiO_2$ . They found that  $TiO_2$  has the least heat transfer while  $Cu$  has the greatest heat transfer. Hayat et al. [13] developed convergent series solution for flow of Casson nanofluids due to a stretching cylinder. They concluded that rate of heat transfer increases for higher values of Brownian motion parameters. Sheikholeslami and Ellahi [14] examined electro-hydrodynamic nanofluid in an enclosure with sinusoidal upper wall. They found that isotherms become denser and heat transfer rate increases with strength of electric field. Sheikholeslami et al. [15] considered Koo-Kleinstreuer-Li (KKL) correlation to investigate flow of nanofluids. Some captivating references are [16–18].

A vast range of research has been done in this area by the researchers. Some are performing experimental studies; some are using

\* Corresponding author.

E-mail address: [ilyaskhan@tdt.edu.vn](mailto:ilyaskhan@tdt.edu.vn) (I. Khan).

<https://doi.org/10.1016/j.rinp.2018.04.007>

Received 9 February 2018; Received in revised form 3 April 2018; Accepted 5 April 2018  
Available online 17 April 2018

2211-3797/ © 2018 The Authors. Published by Elsevier B.V. This is an open access article under the CC BY-NC-ND license (<http://creativecommons.org/licenses/by-nc-nd/4.0/>).

computational work, while few studies have been conducted on analytical side. Halefadel et al. [19] worked on the efficiency of carbon nanotubes water based nanofluids as coolants. They investigated the effect of low nanoparticles volume fraction (ranging from 0.0055% to 0.278%) on density, thermal conductivity and viscosity of nanofluids. Magyari [20] presented a note on homogenous nanofluid models applied to convective heat transfer problems. They used Blasius and Sakiadis forced convection heat transfer problems. Khan [21] studied nanofluids with MoS<sub>2</sub> nanoparticles and found that blade/platelet shapes have the highest heat transfer rate compared to cylinder and brick shapes. The scarcity of fossil fuels induced the researchers to apply a substitute. They found the need to improve the efficiency and performance of solar thermal devices. A comprehensive work has been done to utilize nanoparticles in solar energy applications. Solar collectors are heat exchangers that absorb solar radiation and transfer heat to a fluid passing through it. Tyagi et al. [22] found that the efficiency of collector increases by adding nanoparticles to it. His results show that with variation of volume fraction from 0.1% to 2% and its size the efficiency elevates remarkably. Yousefi et al. [23] experimentally observed that the efficiency of nanofluid (with 0.2% wt.) is greater as compared to water. When they used surfactant in their experiments, they got 15.63% enhancement. The implementations of nanoparticles in solar energy can be found in [24–26] and the references therein.

It is obvious from the above literature that none of them have considered fractional derivatives for nanofluids and its applications in solar energy. Since many researchers have worked on fractional derivatives for viscous fluid which are discussed here. The viscoelastic behavior of material is explained by using fractional calculus. Vieru et al. [27] investigated time fractional free convection flow with Newtonian heating and mass diffusion. They concluded that temperature and velocity are increasing functions of fractional parameter  $\alpha$ . The idea of fractional derivatives has importance not only in mathematics but also in fluid dynamics, applied mathematics electrochemistry, bioengineering, finance and physics (Kulish et al. [28]). Ali et al. [29] applied Caputo-Fabrizio derivatives to MHD free convection flow of generalized Walter-B fluid model. They found thicker momentum boundary layer for larger values of Pr. Azhar et al. [30] concluded that fractional nanofluids have higher heat transfer rate compared to ordinary nanofluids. Imran et al. [31] non-integer order derivative for the flow of Maxwell fluid over oscillating vertical plate. They obtained semi analytical solution using Laplace transform and then used numerical inversion technique Stehfest's and Tzou's algorithm.

With the reference of above literature, no study is reported on fractional derivatives nanofluid area. To best of Authors knowledge, there is very limited work reported in this area very recently by Cao et al. [32] on fractional Maxwell viscoelastic nanofluid over a moving plate. Another study is by Fetecau et al. [33]. They considered Ag and CuO with water as a base fluid. Some recent research work on fractional nanofluids are [34–36] and the references therein. This latest area appealed us to investigate a problem on nanofluids by using fractional derivative model. Our aim here is to find an exact solution of concentration, temperature and velocity field for mixed convection flow of graphene nanofluid past a vertical plate using fractional derivatives. Moreover, to evaluate the heat transfer rate enhancement and examine the physical insight of the problem via graphs.

### Formulation and solution of the problem

Consider Poiseuille flow of water based-nanofluid with graphene nanoparticles in a vertical channel. A uniform magnetic field of strength  $B_0$  is applied in a perpendicular direction to the flow (along  $x$  -axis). External pressure gradient generates mixed convection together with the buoyancy force. The viscous dissipation effect is neglected in the energy equation. In vertical channel,  $T_0$  and  $T_d$  show left and right plate temperatures while  $C_0$  and  $C_d$  shows concentration at left and right plate. The governing equations of momentum, energy and mass are as

under (as in Vieru et al. [27]):

$$\rho_{nf} D_t^\alpha u = -\frac{\partial p}{\partial x} + \mu_{nf} \frac{\partial^2 u}{\partial y^2} - \left( \sigma_{nf} B_0^2 + \frac{\mu_{nf}}{k_1} \right) u + (\rho\beta_T)_{nf} g (T - T_0) + (\rho\beta_c)_{nf} g (C - C_0), \tag{1}$$

$$(\rho c_p)_{nf} D_t^\alpha T = k_{nf} \frac{\partial^2 T}{\partial y^2} + 4\alpha_0^2 (T - T_0), \tag{2}$$

$$D_t^\alpha C = D_{nf} \frac{\partial^2 C}{\partial y^2}, \tag{3}$$

where  $u = u(y,t)$ ,  $T = T(y,t)$ ,  $C = C(y,t)$ ,  $\rho_{nf}$ ,  $\mu_{nf}$ ,  $\sigma_{nf}$ ,  $\beta_T$ ,  $\beta_C$ ,  $g$ ,  $(\rho c_p)_{nf}$ ,  $k_{nf}$ ,  $\alpha_0$ ,  $D_{nf}$ , are respectively fluid velocity in the  $x$  direction, temperature, concentration, density, dynamic viscosity, electrical conductivity of the base fluid, volumetric thermal expansion co-efficient, gravitational acceleration, heat capacitance of nanofluids, thermal conductivity of nanofluid, radiation absorption and thermal diffusion coefficient. Following Makinde and Mhone [1] and Cogley et al. [37], the fluid used is thin with a low density and radiative heat flux given by  $\frac{\partial q_r}{\partial y} = 4\alpha_0^2 (T - T_0)$ . We consider  $-\frac{\partial p}{\partial x} = H(t)[\lambda_0 + \lambda \exp(i\omega t)]$ , with boundary conditions:

$$u(0,t) = 0, \quad u(d,t) = 0, \quad T(0,t) = T_0, \quad T(d,t) = T_d, \\ T(y,0) = T_0, \quad C(0,t) = C_0, \quad C(d,t) = C_d. \tag{4}$$

The density  $\rho_{nf}$ , thermal expansion coefficient  $(\rho\beta)_{nf}$ , heat capacitance  $(\rho c_p)_{nf}$ , thermal conductivity  $k_{nf}$ , electrical conductivity  $\sigma_{nf}$ , and dynamic viscosity  $\mu_{nf}$ , are used as defined (as in Magyari [20]):

$$\rho_{nf} = (1-\phi)\rho_f + \phi\rho_s, \quad k_{nf} = k_f \left( \frac{k_s + 2k_f - 2\phi(k_f - k_s)}{k_s + 2k_f + \phi(k_f - k_s)} \right), \\ (\rho\beta)_{nf} = (1-\phi)(\rho\beta)_f + \phi(\rho\beta)_s, \quad \sigma_{nf} = \sigma_f \left( 1 + \frac{3(\sigma - 1)\phi}{(\sigma + 2) - (\sigma - 1)} \right), \tag{5}$$

$$(\rho c_p)_{nf} = (1-\phi)(\rho c_p)_f + \phi(\rho c_p)_s, \quad \mu_{nf} = \frac{\mu_f}{(1-\phi)^{2.5}},$$

where  $\phi$  is the nanoparticles volume fraction,  $\rho_f$  and  $\rho_s$  is the density of the base fluid and graphene,  $\beta_s$ ,  $\beta_f$ ,  $(c_p)_s$ ,  $(c_p)_f$ ,  $k_s$ ,  $k_f$ , are the volumetric coefficient of thermal expansion, specific heat capacities and thermal conductivities of graphene and base fluid respectively. Using the non-dimensional variables:

$$u^* = \frac{u}{U_0}, \quad x^* = \frac{x}{d}, \quad t^* = \frac{tU_0}{d}, \quad y^* = \frac{y}{d}, \quad p^* = \frac{d}{\mu U_0} p, \quad \lambda_0^* = \frac{\lambda_0 d^2}{\mu U_0}, \quad \lambda^* \\ = \frac{\lambda d^2}{\mu U_0} \quad \theta = \frac{T - T_0}{T_d - T_0}, \quad C^* = \frac{C - C_0}{C_d - C_0}, \quad \omega^* = \frac{\omega d}{U_0}, \quad -\frac{\partial p^*}{\partial x^*} \\ = \lambda_0^* + \lambda^* \exp(i\omega^* t^*), \tag{6}$$

The following non-dimensional differential Eqs. are obtained:

$$\phi_1 Re \frac{\partial u}{\partial t} = H(t)[\lambda_0 + \lambda \exp(i\omega t)] + \phi_2 \frac{\partial^2 u}{\partial y^2} - \left( M + \frac{\phi_2}{K} \right) u + \phi_3 Gr \theta \\ + \phi_4 GmC; \quad y \in [0,1], t \geq 0, \tag{7}$$

$$\phi_5 \frac{Pe}{\lambda_{nf}} \frac{\partial \theta}{\partial t} = \frac{\partial^2 \theta}{\partial y^2} + \frac{N^2}{\lambda_{nf}} \theta, \tag{8}$$

$$Sc \frac{1}{(1-\phi)} \frac{\partial C}{\partial t} = \frac{\partial^2 C}{\partial y^2}, \tag{9}$$

with dimensionless initial and boundary conditions:

$$u(y,0) = 0, \quad u(0,t) = 0, \quad u(1,t) = 0, \\ \theta(y,0) = 0, \quad \theta(0,t) = 0, \quad \theta(1,t) = 1, \\ C(y,0) = 0, \quad C(0,t) = 0, \quad C(1,t) = 1, \tag{10}$$

Where

$$Re = \frac{U_0 d}{\nu}, \quad M = \frac{\sigma_f B_0^2 d^2}{\mu}, \quad K = \frac{k_1}{d^2}, \quad N^2 = \frac{4\alpha_0^2 d^2}{k_f},$$

$$Gr = \frac{g\beta_r d^2 (T_d - T_0)}{\nu U_0}, \quad Gm = \frac{g\beta_C d^2 (C_d - C_0)}{\nu U_0}, \quad Pe = Pr Re. \tag{11}$$

Here we replace the time derivative with time-fractional derivatives to obtain the following fractional differential equations:

$$\phi_1 Re D_t^\alpha u(y,t) = H(t)[\lambda_0 + \lambda \exp(i\omega t)] + \phi_2 \frac{\partial^2 u(y,t)}{\partial y^2} - \left(M + \frac{\phi_2}{K}\right) u(y,t) + \phi_3 Gr \theta(y,t) + \phi_4 Gm C(y,t), \tag{12}$$

$$Pe D_t^\alpha \theta(y,t) = \frac{\partial^2 \theta(y,t)}{\partial y^2} + N^2 \theta(y,t), \tag{13}$$

$$\frac{Sc}{(1-\phi)} D_t^\alpha C(y,t) = \frac{\partial^2 C(y,t)}{\partial y^2}, \tag{14}$$

where  $D_t^\alpha u(y,t)$  represent the Caputo time-fractional derivative of  $u(y,t)$ , defined as:

$$D_t^\alpha u(y,t) = \begin{cases} \frac{1}{\Gamma(1-\alpha)} \int_0^t \frac{1}{(t-\tau)^\alpha} \frac{\partial u(y,\tau)}{\partial \tau} d\tau; & 0 < \alpha < 1, \\ \frac{\partial u(y,t)}{\partial t}; & \alpha = 1. \end{cases} \tag{15}$$

**Solution of the problem**

To obtain solutions of the Eqs. (12)–(14) using Eq. (10), we use Laplace transform w.r.t the variable  $t$ .

**Temperature field**

Applying the Laplace transform to Eq. (13) and using Eq. (10), we obtain the problem in transform domain

$$(b_0 q^\alpha - b_1^2) \bar{\theta}(y,q) = \frac{\partial^2 \bar{\theta}(y,q)}{\partial y^2}, \tag{16}$$

$$\bar{\theta}(0,q) = 0, \bar{\theta}(1,q) = \frac{1}{q}, \tag{17}$$

with solution:

$$\bar{\theta}(y,q) = \frac{\sinh \left[ y \sqrt{b_0} \sqrt{q^\alpha - \frac{b_1^2}{b_0}} \right]}{q \sinh \left[ \sqrt{b_0} \sqrt{q^\alpha - \frac{b_1^2}{b_0}} \right]} \tag{18}$$

To obtain the inverse Laplace, we rewrite Eq. (18) in the form

$$\bar{\theta}(y,q) = \frac{1}{q^{1-\alpha}} \frac{\sinh \left[ y \sqrt{b_0} \sqrt{q^\alpha - \frac{b_1^2}{b_0}} \right]}{q^\alpha \sinh \left[ \sqrt{b_0} \sqrt{q^\alpha - \frac{b_1^2}{b_0}} \right]} \tag{19}$$

Using (A2) from Appendix, the convolution theorem, and the formula

$$L^{-1} \left\{ \frac{1}{q^{1-\alpha}} \right\} = \begin{cases} \frac{t^{-\alpha}}{\Gamma(1-\alpha)}, & 0 < \alpha < 1, \\ \delta(t), & \alpha = 1, \end{cases} \tag{20}$$

For  $0 < \alpha < 1$ , we obtain

$$\theta(y,t) = \int_0^t \frac{(t-\tau)^{-\alpha}}{\Gamma(1-\alpha)} h(y\sqrt{b_0}, \tau, \frac{b_1}{b_0}, \sqrt{b_0}) d\tau = \int_0^t \frac{(t-\tau)^{-\alpha}}{\Gamma(1-\alpha)} \int_0^\infty \tau^{-1} f(y\sqrt{b_0}, u, -\frac{b_1}{b_0}, \sqrt{b_0}) \phi(0, -\alpha, -u\tau^{-\alpha}) du d\tau = \int_0^\infty f(y\sqrt{b_0}, u, -\frac{b_1}{b_0}, \sqrt{b_0}) \int_0^t \frac{(t-\tau)^{-\alpha}}{\Gamma(1-\alpha)} \tau^{-1} \phi(0, -\alpha, -u\tau^{-\alpha}) d\tau du. \tag{21}$$

where  $h$  and  $f$  are defined in Appendix.

To express the temperature field in terms of Wright function, we

consider the function image  $V(q) = \frac{1}{q} e^{-aq^\sigma}, a \geq 0, 0 < \sigma < 1$  with inverse Laplace transform

$$v(t) = L^{-1}\{V(q)\}(t) = \phi(1, -\sigma; -at^{-\sigma}),$$

Since

$$v(0) = \lim_{t \rightarrow 0^+} v(t) = \lim_{q \rightarrow \infty} qV(q) = \lim_{q \rightarrow \infty} q \frac{1}{q} e^{-aq^\sigma} = 0.$$

$$L\{v'(t)\} = qV(q) - V(0) = qV(q) = q \frac{1}{q} e^{-aq^\sigma} - 0 = e^{-aq^\sigma}$$

$$v'(t) = L^{-1}\{e^{-aq^\sigma}\} = t^{-1} \phi(0, -\sigma, -at^{-\sigma})$$

Therefore

$$t^{-1} \phi(0, -\sigma, -at^{-\sigma}) = \frac{d\Phi(1, -\sigma, -at^{-\sigma})}{dt} \tag{22}$$

Using Eq. (20), we have

$$\int_0^t \frac{(t-\tau)^{-\alpha}}{\Gamma(1-\alpha)} \tau^{-1} \phi(0, -\alpha, -u\tau^{-\alpha}) d\tau = D_t^\alpha \Phi(1, -\alpha, -ut^{-\alpha}),$$

and Eq. (21), becomes

$$\theta(y,t) = \int_0^\infty f(y\sqrt{b_0}, u, -\frac{b_1}{b_0}, \sqrt{b_0}) D_t^\alpha \Phi(1, -\alpha, -ut^{-\alpha}) du; \quad 0 < \alpha < 1. \tag{23}$$

For  $\alpha = 1$

$$\theta(y,t) = f(y\sqrt{b_0}, u, -\frac{b_1}{b_0}, \sqrt{b_0}). \tag{24}$$

**Concentration field**

Using Eqs. (10) and (14), we obtain the following problem in transform domain  $\bar{C}(y,q)$ :

$$b_3 q^\alpha C(y,t) = \frac{\partial^2 C(y,t)}{\partial y^2}, \tag{25}$$

Where  $b_3 = \frac{Sc}{(1-\phi)}$ ,

$$\bar{C}(0,q) = 0, \quad \bar{C}(1,q) = \frac{1}{q}. \tag{26}$$

The solution of the problem is

$$\bar{C}(y,q) = \frac{\sinh[y\sqrt{b_3} \sqrt{q^\alpha}]}{q \sinh[\sqrt{b_3} \sqrt{q^\alpha}]} \tag{27}$$

To obtain the inverse Laplace of Eq. (27), we rewrite this function in the form

$$\bar{C}(y,q) = \frac{1}{q^{1-\alpha}} \frac{\sinh[y\sqrt{b_3} \sqrt{q^\alpha}]}{q^\alpha \sinh[\sqrt{b_3} \sqrt{q^\alpha}]} \tag{28}$$

After applying inverse Laplace transform, using the formula (20), (A2) from the Appendix and convolution theorem:

$$C(y,t) = \int_0^t \frac{(t-\tau)^{-\alpha}}{\Gamma(1-\alpha)} h(y\sqrt{b_3}, \tau, 0, \sqrt{b_3}) d\tau \tag{29}$$

It can be written as:

$$C(y,t) = \int_0^t \frac{(t-\tau)^{-\alpha}}{\Gamma(1-\alpha)} \int_0^\infty \tau^{-1} f(y\sqrt{b_3}, \tau, 0, \sqrt{b_3}) \phi(0, -\alpha, -u\tau^{-\alpha}) du d\tau = \int_0^\infty f(y\sqrt{b_3}, \tau, 0, \sqrt{b_3}) \int_0^t \frac{(t-\tau)^{-\alpha}}{\Gamma(1-\alpha)} \tau^{-1} \phi(0, -\alpha, -u\tau^{-\alpha}) d\tau du. \tag{30}$$

In the form of Caputo fractional derivative of the Wright function, it becomes:

$$C(y,t) = \int_0^\infty f(y\sqrt{b_3}, u, 0, \sqrt{b_3}) D_t^\alpha \Phi(1, -\alpha, -ut^{-\alpha}) du; 0 < \alpha < 1. \tag{31}$$

**Velocity field**

Using Eqs. (10) and (28), we obtain the following problem in transform domain for the velocity  $\bar{u}(y,q)$ :

$$(\phi_1 \text{Re}q^\alpha + M + \frac{\phi_2}{K})\bar{u}(y,q) = \phi_2 \frac{\partial^2 \bar{u}(y,q)}{\partial y^2} + \phi_3 Gr \frac{\sinh[y\sqrt{b_0}\sqrt{q^\alpha + b_2}]}{q \sinh[\sqrt{b_0}\sqrt{q^\alpha + b_2}]} + \phi_4 Gm \frac{\sinh[y\sqrt{b_3}\sqrt{q^\alpha}]}{q \sinh[\sqrt{b_3}\sqrt{q^\alpha}]} + \frac{\lambda_0}{q} + \frac{\lambda}{q-i\omega}, \tag{32}$$

$$\bar{u}(0,q) = 0, \quad \bar{u}(1,q) = 0. \tag{33}$$

We introduce notations:

$$a_0 = \frac{1}{\text{Re}} \left( M + \frac{\phi_2}{K} \right), \quad b_2 = -\frac{b_1^2}{b_0}.$$

Particular solution of Eq. (32), is

$$\begin{aligned} \bar{u}_p(y,q) = & \frac{a_2}{(a_1-b_0)(q^\alpha + c_0)} \frac{\sinh[y\sqrt{b_0}\sqrt{q^\alpha + b_2}]}{q \sinh[\sqrt{b_0}\sqrt{q^\alpha + b_2}]} \\ & + \frac{a_3}{(a_1-b_3)(q^\alpha + d_0)} \frac{\sinh[y\sqrt{b_3}\sqrt{q^\alpha}]}{q \sinh[\sqrt{b_3}\sqrt{q^\alpha}]} \\ & + \frac{a_4}{a_1(q^\alpha + a_0)} \left( \frac{\lambda_0}{q} + \frac{\lambda}{q-i\omega} \right). \end{aligned} \tag{34}$$

Complementary solution of the homogeneous equation associated with Eq. (32), is

$$\bar{u}_c(y,q) = C_1 \sinh(y\sqrt{a_1}\sqrt{q^\alpha + a_0}) + C_2 \cosh(y\sqrt{a_1}\sqrt{q^\alpha + a_0}). \tag{35}$$

The general solution of Eq. (32) is

$$\begin{aligned} \bar{u}(y,q) = & C_1 \sinh(y\sqrt{a_1}\sqrt{q^\alpha + a_0}) + C_2 \cosh(y\sqrt{a_1}\sqrt{q^\alpha + a_0}) \\ & + \frac{a_2}{(a_1-b_0)(q^\alpha + c_0)} \frac{\sinh[y\sqrt{b_0}\sqrt{q^\alpha + b_2}]}{q \sinh[\sqrt{b_0}\sqrt{q^\alpha + b_2}]} \\ & + \frac{a_3}{(a_1-b_3)(q^\alpha + d_0)} \frac{\sinh[y\sqrt{b_3}\sqrt{q^\alpha}]}{q \sinh[\sqrt{b_3}\sqrt{q^\alpha}]} \\ & + \frac{a_4}{a_1(q^\alpha + a_0)} \left( \frac{\lambda_0}{q} + \frac{\lambda}{q-i\omega} \right) \end{aligned} \tag{36}$$

Using Eq. (33), we obtain the solution of  $\bar{u}(y,q)$  as

$$\begin{aligned} \bar{u}(y,q) = & \frac{q^\alpha}{a_1(q^\alpha + a_0)} \left( \frac{\lambda_0}{q} \right. \\ & \left. + \frac{\lambda}{q-i\omega} \right) \frac{a_4 \cosh[\sqrt{a_1}\sqrt{q^\alpha + a_0}] \sinh[y\sqrt{a_1}\sqrt{q^\alpha + a_0}]}{q^\alpha \sinh[\sqrt{a_1}\sqrt{q^\alpha + a_0}]} \\ & - \frac{a_2}{(a_1-b_0)(q^\alpha + c_0)} \frac{q^\alpha \sinh[y\sqrt{a_1}\sqrt{q^\alpha + a_0}]}{q \sinh[\sqrt{a_1}\sqrt{q^\alpha + a_0}]} \\ & - \frac{a_3}{(a_1-b_3)(q^\alpha + d_0)} \frac{q^\alpha \sinh[y\sqrt{a_1}\sqrt{q^\alpha + a_0}]}{q \sinh[\sqrt{a_1}\sqrt{q^\alpha + a_0}]} \\ & - \left( \frac{\lambda_0}{q} + \frac{\lambda}{q-i\omega} \right) \frac{a_4 \sinh[y\sqrt{a_1}\sqrt{q^\alpha + a_0}]}{a_1(q^\alpha + a_0) \sinh[\sqrt{a_1}\sqrt{q^\alpha + a_0}]} \\ & - \frac{a_4 \cosh[y\sqrt{a_1}\sqrt{q^\alpha + a_0}]}{a_1(q^\alpha + a_0)} \left( \frac{\lambda_0}{q} + \frac{\lambda}{q-i\omega} \right) \\ & + \frac{a_2}{q(a_1-b_0)} \frac{q^\alpha \sinh[y\sqrt{b_0}\sqrt{q^\alpha + b_2}]}{(q^\alpha + c_0) q \sinh[\sqrt{b_0}\sqrt{q^\alpha + b_2}]} \\ & + \frac{a_3 q^\alpha}{q(a_1-b_3)(q^\alpha + d_0)} \frac{\sinh[y\sqrt{b_3}\sqrt{q^\alpha}]}{q \sinh[\sqrt{b_3}\sqrt{q^\alpha}]} \\ & + \frac{a_4}{a_1(q^\alpha + a_0)} \left( \frac{\lambda_0}{q} + \frac{\lambda}{q-i\omega} \right). \end{aligned} \tag{37}$$

Taking Inverse Laplace transform of Eq. (37) and using (A1) from the Appendix:

$$\begin{aligned} u(y,t) = & (\lambda_0 + \lambda e^{i\omega t}) \left[ \frac{1}{2} \psi[(y+1),t] + \frac{1}{2} \psi[(y-1),t] \right] \\ & - a_4 \int_0^\infty \left\{ \sum_{n=0}^\infty \left[ \text{erfc} \left( \frac{1-y+2n}{2\sqrt{u}} \right) \right] - \text{erfc} \left( \frac{1+y+2n}{2\sqrt{u}} \right) \right\} \frac{e^{a_0 a_1 u t^{-1}} \Phi(0, -\alpha, -a_1 u t^{-\frac{\alpha}{2}})}{du} \\ & - \frac{a_1 a_2}{(a_1-b_0)} (1 + (a_0 - c_0) t^\alpha E_{\alpha,\alpha+1}(-c_0 t^\alpha)) \\ & \int_0^\infty \left\{ \sum_{n=0}^\infty \left[ \text{erfc} \left( \frac{1-y+2n}{2\sqrt{u}} \right) \right] - \text{erfc} \left( \frac{1+y+2n}{2\sqrt{u}} \right) \right\} \frac{e^{a_0 a_1 u t^{-1}} \Phi(0, -\alpha, -a_1 u t^{-\frac{\alpha}{2}})}{du} \\ & - \frac{a_1 a_3}{(a_1-b_3)} (1 + (a_0 - d_0) t^\alpha E_{\alpha,\alpha+1}(-d_0 t^\alpha)) \\ & \int_0^\infty \left\{ \sum_{n=0}^\infty \left[ \text{erfc} \left( \frac{1-y+2n}{2\sqrt{u}} \right) \right] - \text{erfc} \left( \frac{1+y+2n}{2\sqrt{u}} \right) \right\} \frac{e^{a_0 a_1 u t^{-1}} \Phi(0, -\alpha, -a_1 u t^{-\frac{\alpha}{2}})}{du} \\ & - a_4 (\lambda_0 + \lambda e^{i\omega t}) \frac{1}{2} \left[ \int_0^\infty (2 - \text{erfc} \frac{y}{2\sqrt{u}}) g(u,t) du \right. \\ & \left. + \int_0^\infty \text{erfc} \frac{y}{2\sqrt{u}} g(u,t) du \right] + \frac{a_2 b_0}{(a_1-b_0)} (1 + (b_2 - c_0) t^\alpha E_{\alpha,\alpha+1}(-c_0 t^\alpha)) + \frac{a_3}{(a_1-b_3)} F_{\alpha,\alpha-1}(t, -d_0) \sum_{n=0}^\infty \left[ \text{erfc} \left( \frac{1-y+2n}{2\sqrt{b_3 t}} \right) - \text{erfc} \left( \frac{1+y+2n}{2\sqrt{b_3 t}} \right) \right] + \frac{a_4}{a_1} F_\alpha(t, -a_0) (\lambda_0 + \lambda e^{i\omega t}). \end{aligned} \tag{38}$$

**Nusselt number, Sherwood’s number and skin friction**

The entity of physical interest and applications Nusselt number, Sherwood’s Number and Skin friction are evaluated. Nusselt number gives the information about heat transfer rate of the fractional nano-fluid at the walls. First, we find Nusselt number  $Nu_u(t)$  at wall  $y = 0$ :

$$Nu_u(t) = \frac{d}{k_f} \frac{q_w}{(T_d - T_0)} = -\frac{d}{k_f} \frac{k_{nf}}{(T_d - T_0)} \frac{\partial T(y,t)}{\partial y} \Big|_{y=0} = -\frac{k_{nf}}{k_f} \frac{\partial \theta(y,t)}{\partial y} \Big|_{y=0}, \tag{39}$$

$$\begin{aligned} Nu_u(t) = & -\frac{k_{nf}}{k_f} L^{-1} \left\{ \frac{\sqrt{b_0}\sqrt{q^\alpha + b_2}}{q} \frac{1}{\sinh(\sqrt{b_0}\sqrt{q^\alpha + b_2})} \right\} \\ = & -\frac{k_{nf}}{k_f} L^{-1} \left\{ \frac{\sqrt{b_0}\sqrt{q^\alpha + b_2}}{q} \sum_{n=0}^\infty \frac{\exp(-\sqrt{b_0}(2n+1)\sqrt{q^\alpha + b_2})}{\sqrt{q^\alpha + b_2}} \right\}, \end{aligned} \tag{40}$$

Let  $C_n(q) = \sum_{n=0}^\infty \frac{\exp(-\sqrt{b_0}(2n+1)\sqrt{q^\alpha + b_2})}{\sqrt{q^\alpha + b_2}}$ ,  $D_n(q) = \sqrt{b_0} \frac{q^\alpha + b_2}{q}$ . Their inverse Laplace transform are:

$$\begin{aligned} C_n(t) = & \int_0^\infty \frac{1}{\sqrt{\pi z}} \exp\left(\frac{-b_0(2n+1)^2}{4z} - b_0 z\right) t^{-1} \phi(0, -\alpha, -z t^{-\alpha}) dz, \\ D_n(t) = & \sqrt{b_0} \left[ \frac{t^{-\alpha}}{\Gamma(1-\alpha)} + b_2 \right], \quad 0 < \alpha < 1, \end{aligned}$$

Thus, the Nusselt number is:

$$Nu_u(t) = -\frac{k_{nf}}{k_f} (D_n(t) * \sum_{n=0}^\infty C_n(t)) = -\frac{k_{nf}}{k_f} \sum_{n=0}^\infty \int_0^\infty D_n(t-\tau) C_n(\tau) d\tau. \tag{41}$$

Now we find Nusselt number  $Nu_2(t)$  at wall  $y = 0$ , which is given by

$$Nu_2(t) = -\frac{k_{nf}}{k_f} L^{-1} \left\{ \sqrt{b_0} \frac{q^\alpha + b_2 \cosh(\sqrt{b_0} \sqrt{q^\alpha + b_2})}{q \sinh(\sqrt{b_0} \sqrt{q^\alpha + b_2})} \right\}$$

$$= -\frac{k_{nf}}{k_f} L^{-1} \left\{ \sqrt{b_0} \frac{q^\alpha + b_2}{q} \sum_{n=0}^{\infty} \frac{\exp(-2n\sqrt{b_0} \sqrt{q^\alpha + b_2}) + \exp(-2(n+1)\sqrt{b_0} \sqrt{q^\alpha + b_2})}{\sqrt{q^\alpha + b_2}} \right\}. \tag{42}$$

The inverse Laplace transform of

$$G_n(q) = \sum_{n=0}^{\infty} \frac{\exp(-2n\sqrt{b_0} \sqrt{q^\alpha + b_2}) + \exp(-2(n+1)\sqrt{b_0} \sqrt{q^\alpha + b_2})}{\sqrt{q^\alpha + b_2}},$$

is

$$G_n(t) = \int_0^\infty \frac{1}{\sqrt{\pi z}} \left[ \exp\left(\frac{-n^2 b_0}{z} - b_0 z\right) + \exp\left(\frac{-(n+1)^2 b_0}{z} - b_0 z\right) \right] t^{-1} \phi(0, -\alpha; -z t^{-\alpha}) dz.$$

The Nusselt number is:

$$Nu_2(t) = -\frac{k_{nf}}{k_f} (D_n(t) * \sum_{n=0}^{\infty} G_n(t)) = -\frac{k_{nf}}{k_f} \sum_{n=0}^{\infty} \int_0^\infty D_n(t-\tau) G_n(\tau) d\tau. \tag{43}$$

For ordinary nanofluid  $\alpha = 1$ , the property of Wright function  $t^{-1} \phi(0, -1, -z t^{-1}) = \delta(t-z)$ , Eqs. (41) and (43) become:

$$Nu_{h1}(t) = -\frac{k_{nf}}{k_f} \left( \sum_{n=0}^{\infty} \sqrt{b_0} [\delta(t) + b_2] * \frac{1}{\sqrt{\pi t}} \exp\left(\frac{-b_0(2n+1)^2}{4t} - b_0 t\right) \right)$$

$$= -\frac{k_{nf}}{k_f} \sum_{n=0}^{\infty} \frac{\sqrt{b_0}}{\sqrt{\pi t}} \exp\left(\frac{-b_0(2n+1)^2}{4t} - b_0 t\right)$$

$$+ \sum_{n=0}^{\infty} b_2 \sqrt{b_0} \int_0^t \frac{1}{\sqrt{\pi t}} \exp\left(\frac{-b_0(2n+1)^2}{4t} - b_0 \tau\right) d\tau$$

$$= -\frac{k_{nf}}{k_f} \sum_{n=0}^{\infty} \frac{\sqrt{b_0}}{\sqrt{\pi t}} \exp\left(\frac{-b_0(2n+1)^2}{4t} - b_0 t\right) + \sqrt{b_2 b_0} \zeta(t), \tag{44}$$

Where

$$\zeta(t) = \frac{1}{2} \sum_{n=0}^{\infty} \left[ e^{-(2n+1)\sqrt{b_0 b_2}} \operatorname{erfc}\left(\frac{(2n+1)\sqrt{b_0}}{2\sqrt{t}} - \sqrt{b_2 t}\right) - e^{-(2n+1)\sqrt{b_0 b_2}} \operatorname{erfc}\left(\frac{(2n+1)\sqrt{b_0}}{2\sqrt{t}} + \sqrt{b_2 t}\right) \right], \tag{45}$$

$$Nu_2(t) = -\frac{k_{nf}}{k_f} \left[ \frac{\sqrt{b_0}}{\sqrt{\pi}} \zeta(t) + b_2 \frac{\sqrt{b_0}}{\sqrt{\pi}} \int_0^t \zeta(\tau) d\tau \right], \tag{46}$$

with

$$\zeta(t) = \sum_{n=0}^{\infty} t^{-\frac{1}{2}} \left[ \exp\left(\frac{-n^2 \sqrt{b_0}}{t} - b_2 t\right) + \exp\left(\frac{-(n+1)^2 \sqrt{b_0}}{t} - b_2 t\right) \right].$$

Now we find Sherwood's number which is given by:

$$Sh(t) = \frac{dq_m}{D_f(C_d - C_0)}, \tag{47}$$

where:  $q_m = -D_{nf} \left( \frac{\partial C}{\partial y} \right) \Big|_{y=0}$  is the mass flux.

$$Sh_h(t) = \frac{-D_{nf} d}{D_f(C_d - C_0)} \left( \frac{\partial C}{\partial y} \right) \Big|_{y=0} = -(1-\phi) L^{-1} \left\{ \left( \frac{\partial \bar{C}}{\partial y} \right) \Big|_{y=0} \right\}$$

$$= -(1-\phi) L^{-1} \left\{ \frac{\sqrt{b_3} \sqrt{q^\alpha}}{q \sinh[\sqrt{b_3} \sqrt{q^\alpha}]} \right\} \tag{48}$$

Let

$$\bar{Q}(q) = \frac{1}{q^{1-\alpha}}, \bar{R}(q) = \frac{\sqrt{b_3}}{\sqrt{q^\alpha} \sinh[\sqrt{b_3} \sqrt{q^\alpha}]} = \sqrt{b_3} \sum_{n=0}^{\infty} \frac{\exp(-\sqrt{b_3} (2n+1) \sqrt{q^\alpha})}{\sqrt{q^\alpha}}. \text{we have}$$

**Table 1**

Thermophysical properties of base fluid and graphene nanoparticles.

Physical properties	Water	Graphene
$\rho/\text{kgm}^{-3}$	997	2250
$c_p/\text{Jkg}^{-1}\text{K}^{-1}$	4197	2100
$k/\text{Wm}^{-1}\text{K}^{-1}$	0.613	2500
$\sigma/\text{Sm}^{-1}$	0.005	$10^7$

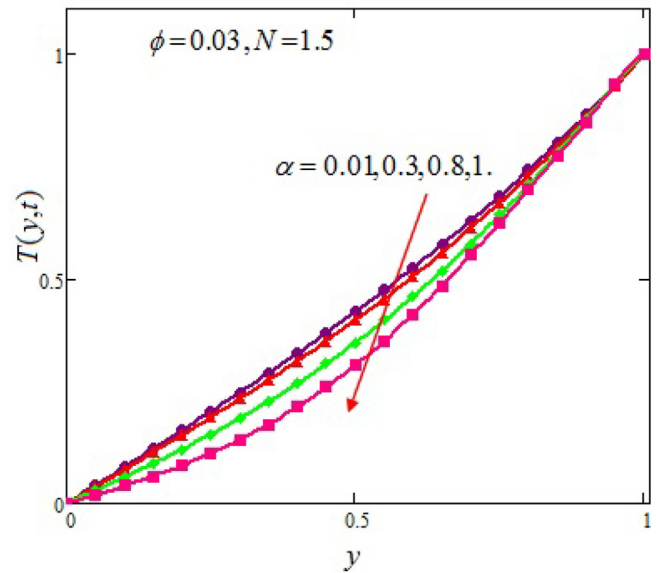


Fig. 1. Temperature profile for different values of fractional parameter  $\alpha$ .

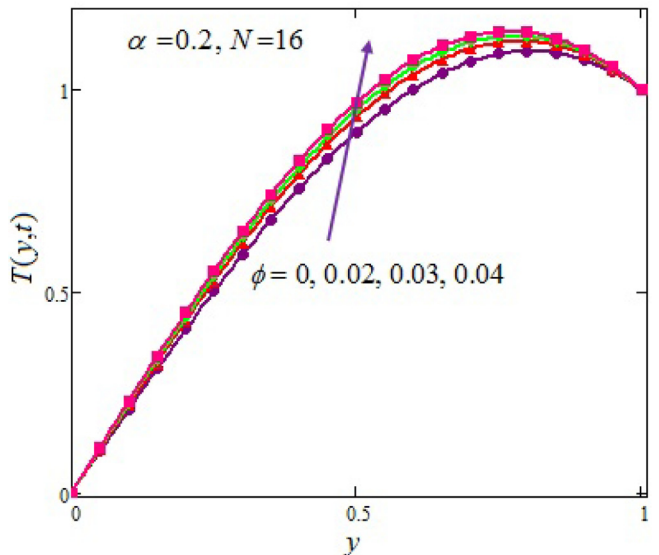


Fig. 2. Temperature profile for different values of volume fraction  $\phi$  for fractional nanofluid.

$$Q(t) = \frac{t^{-\alpha}}{\Gamma(1-\alpha)}, R(t) = \int_0^\infty \frac{1}{\pi z} \exp\left(\frac{-b_3(2n+1)^2}{4z}\right) t^{-1} \phi(0, -\alpha; -z t^{-\alpha}) dz,$$

Thus Eq. (48) becomes:

$$Sh_h(t) = \sqrt{b_3} \left[ Q(t) * \sum_{n=0}^{\infty} R(t) \right] = \sqrt{b_3} \sum_{n=0}^{\infty} \int_0^\infty Q(t-\tau) R(\tau) d\tau, \tag{49}$$

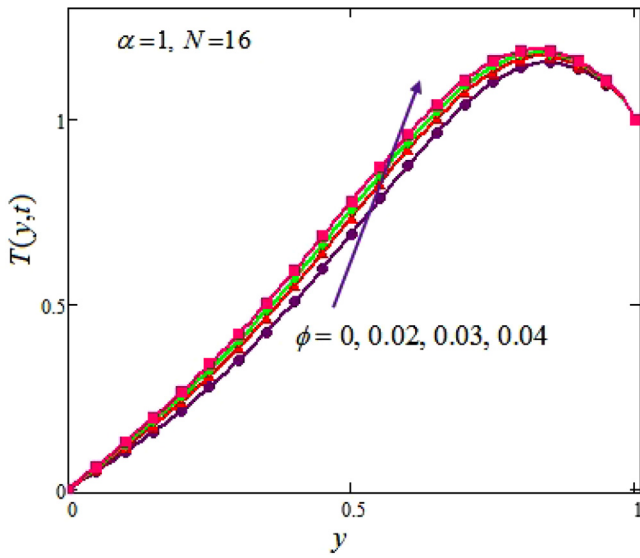


Fig. 3. Temperature profile for different values of volume fraction  $\phi$  for ordinary nanofluid.

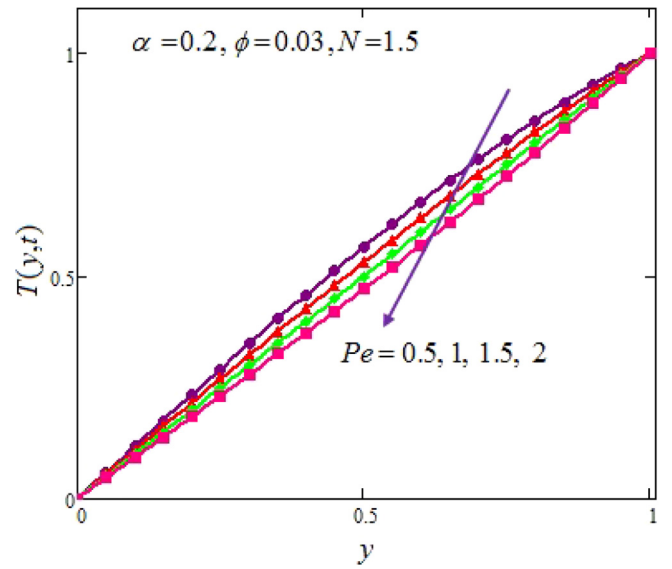


Fig. 5. Temperature profile for different values of Peclet number  $Pe$ .

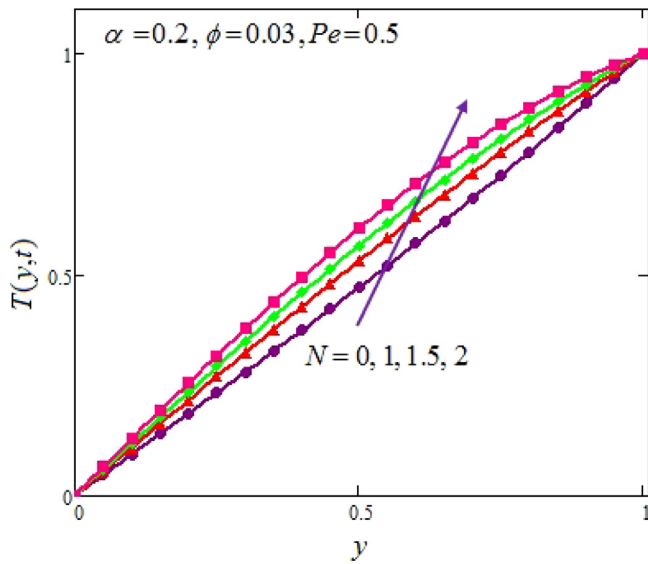


Fig. 4. Temperature profile for different values of radiation parameter  $N$  for ordinary nanofluid.

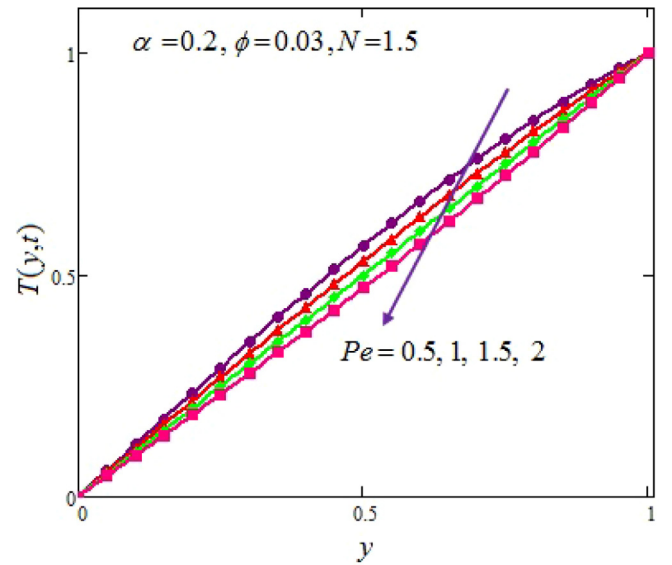


Fig. 6. Concentration profile for different values of Schmidt number  $Sc$ .

$$Sh_2(t) = -(1-\phi)L^{-1} \left\{ \left( \frac{\partial \bar{C}}{\partial y} \right) \Big|_{y=1} \right\} = \sqrt{b_3} \left[ Q(t) * \sum_{n=0}^{\infty} S(t) \right]$$

$$= -(1-\phi)\sqrt{b_3} \sum_{n=0}^{\infty} \int_0^{\infty} Q(t-\tau)S(\tau) d\tau, \tag{50}$$

where

$$S(t) = \int_0^{\infty} \frac{1}{\pi z} \exp\left(\frac{-n^2 b_3}{z}\right) + \exp\left(\frac{-(n+1)b_3}{z}\right) t^{-1} \phi(0, -\alpha; -z t^{-\alpha}) dz.$$

Now Skin friction on the walls is evaluated as:

$$Cf_1(t) = \frac{\bar{\tau}_w}{\rho_f \left(\frac{v_f^2}{d}\right)} = \frac{\mu_{nf} \bar{\tau}_w}{\rho_f \left(\frac{v_f^2}{d}\right)} \left( \frac{\partial u(y,t)}{\partial y} \right) \Big|_{y=0}$$

$$= \frac{\mu_{nf}}{\mu_f} \left( \frac{\partial u(y,t)}{\partial y} \right) \Big|_{y=0} = \frac{1}{(1-\phi)^{2.5}} \lim_{y \rightarrow 0^+} L^{-1} \left\{ \frac{\partial \bar{u}(y,q)}{\partial y} \right\}, \tag{51}$$

$$Cf_1(t) = \frac{1}{(1-\phi)^{2.5}} L^{-1} \left\{ \frac{\partial \bar{u}(y,q)}{\partial y} \Big|_{y=0} \right\}$$

$$= \frac{1}{(1-\phi)^{2.5}} \left\{ \begin{aligned} & \frac{a_4}{\sqrt{a_1}} (\lambda_0 + \lambda e^{i\omega t}) * \sum_{n=0}^{\infty} J_n(t) - \frac{a_2 \sqrt{a_1}}{(a_1 - b_0)} (1 \\ & + (a_0 - c_0) t^\alpha E_{\alpha, \alpha+1}(-c_0 t^\alpha)) * \sum_{n=0}^{\infty} K_n(t) \\ & - \frac{a_3}{(a_1 - b_3)} (1 + (a_0 - d_0) t^\alpha E_{\alpha, \alpha+1}(-d_0 t^\alpha)) * \sum_{n=0}^{\infty} K_n(t) \\ & - \frac{a_4}{\sqrt{a_1}} (\lambda_0 + \lambda e^{i\omega t}) \sum_{n=0}^{\infty} K_n(t) + \frac{a_2 \sqrt{b_0}}{(a_1 - b_0)} (1 \\ & + (b_2 - c_0) t^\alpha E_{\alpha, \alpha+1}(-c_0 t^\alpha)) * \sum_{n=0}^{\infty} L_n(t) \\ & + \frac{a_3 \sqrt{b_3}}{(a_1 - b_3)} R_{\alpha, \alpha-1}(t - d_0) * \sum_{n=0}^{\infty} M_n(t) \end{aligned} \right\}, \tag{52}$$

Where

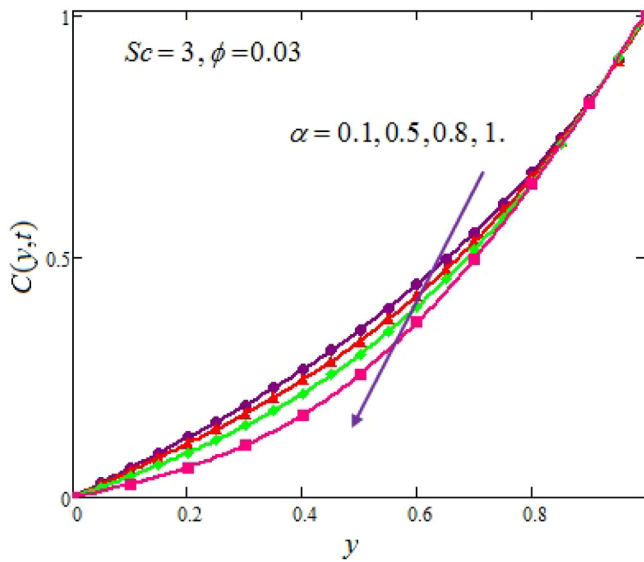


Fig. 7. Concentration profile for different values of fractional parameter  $\alpha$ .

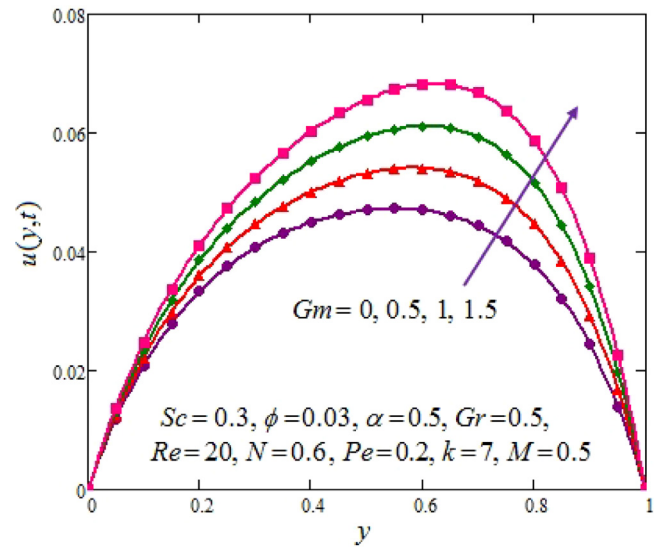


Fig. 9. Velocity profile for different values of Solutal Grashof number  $Gm$ .

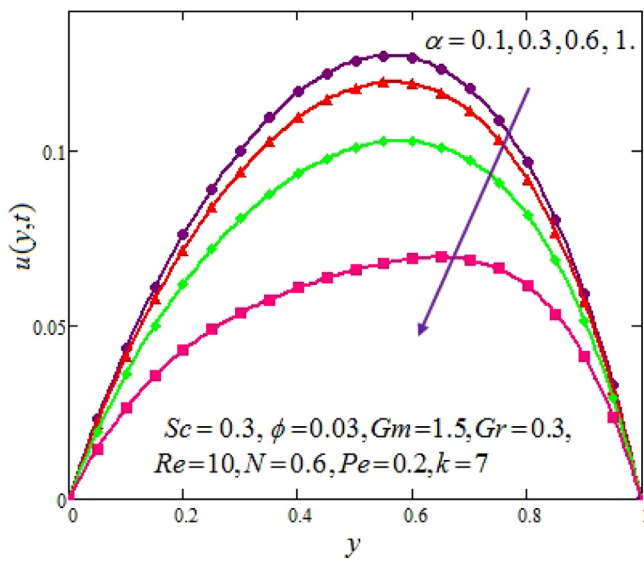


Fig. 8. Velocity profile for different values of fractional parameter  $\alpha$ .

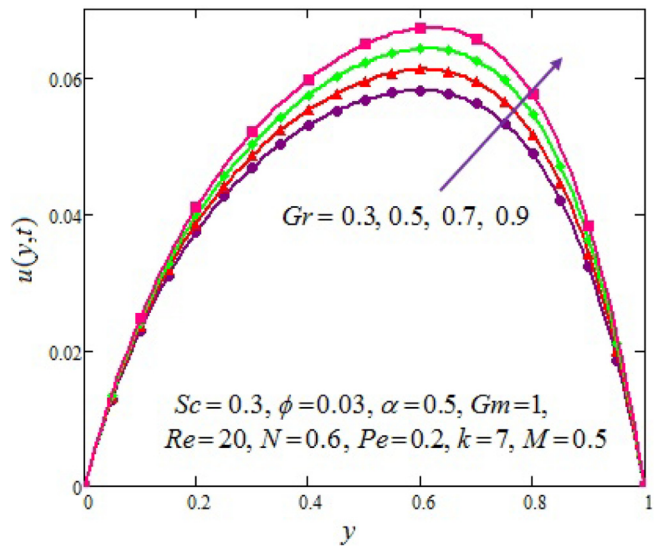


Fig. 10. Velocity profile for different values of Grashof number  $Gr$ .

$$J_n(t) = \int_0^\infty \frac{1}{\pi z} \exp\left(\frac{-n^2 a_1}{z} - a_0 z\right) + \exp\left(\frac{-(n+1)a_1}{z}\right) t^{-1} \phi(0, -\alpha; -zt^{-\alpha}) dz$$

$$K_n(t) = \int_0^\infty \frac{1}{\pi z} \exp\left(\frac{-a_1(2n+1)^2}{4z} - a_0 z\right) t^{-1} \phi(0, -\alpha; -zt^{-\alpha}) dz$$

$$L_n(t) = \int_0^\infty \frac{1}{\pi z} \exp\left(\frac{-b_0(2n+1)^2}{4z} - b_2 z\right) t^{-1} \phi(0, -\alpha; -zt^{-\alpha}) dz$$

$$M_n(t) = \int_0^\infty \frac{1}{\pi z} \exp\left(\frac{-b_3(2n+1)^2}{4z}\right) t^{-1} \phi(0, -\alpha; -zt^{-\alpha}) dz$$

**Graphical results and discussion**

A brief analysis is made on the effect of MHD mixed convection Poiseuille flow of graphene nanofluid inside a vertical channel in a porous medium. Solutions of temperature, concentration, velocity field and Nusselt number of practical interest are acquired. Keeping some of the embedded parameters fixed while varying others show the behavior

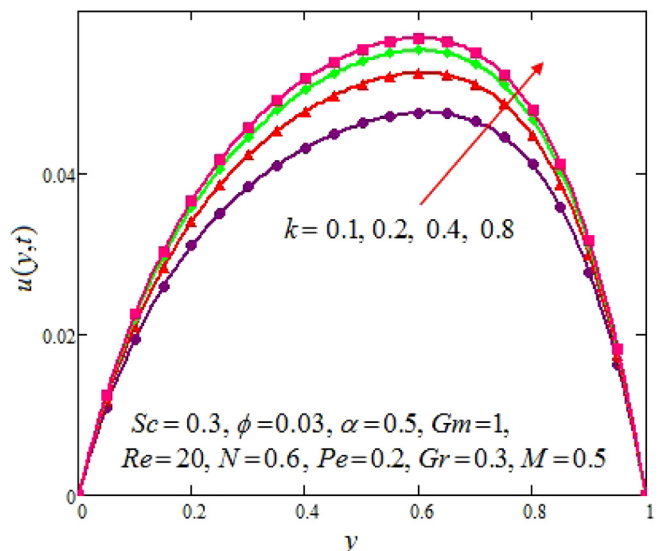


Fig. 11. Velocity profile for different values of Permeability parameter  $k$ .

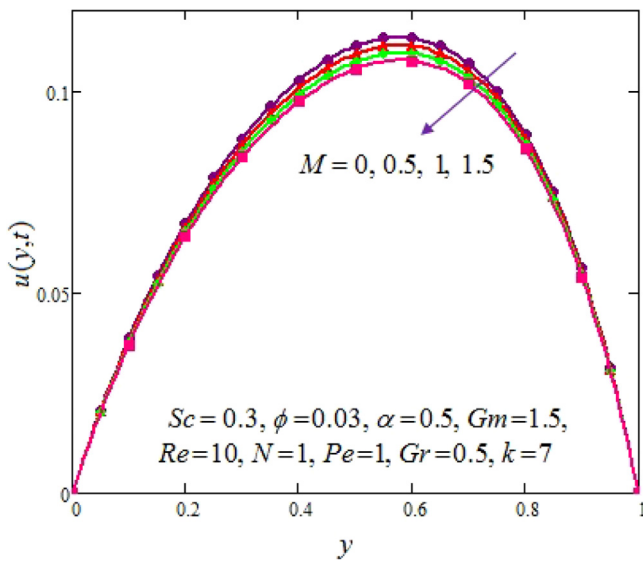


Fig. 12. Velocity profile for different values of Magnetic parameter  $M$ .

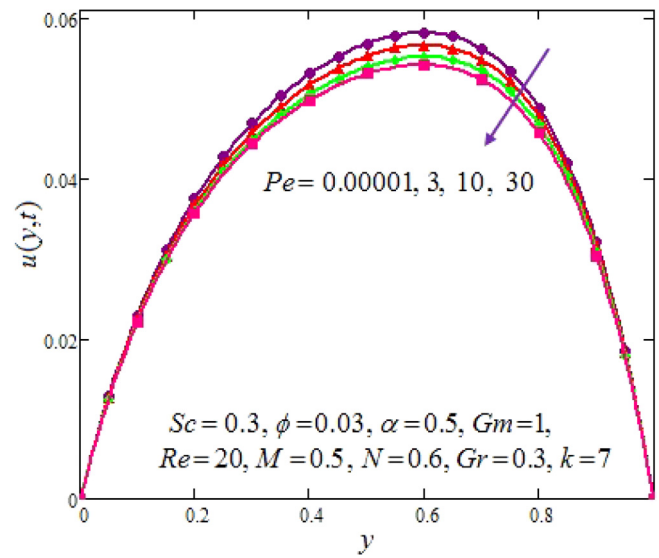


Fig. 14. Velocity profile for different values of Peclet number  $Pe$ .

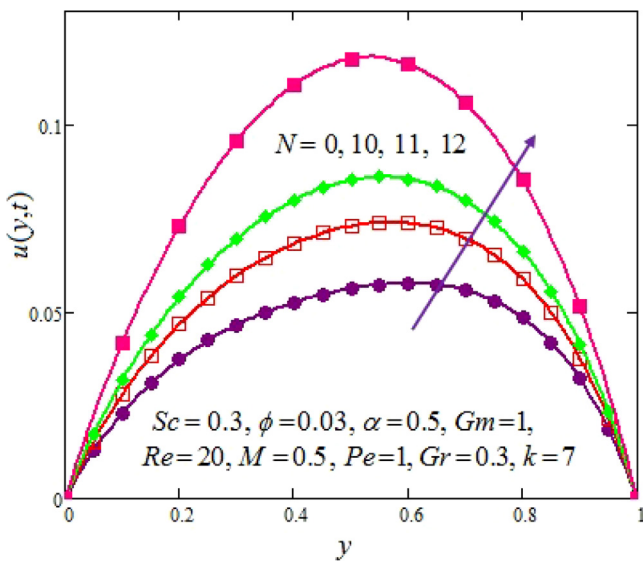


Fig. 13. Velocity profile for different values of Radiation parameter  $N$ .

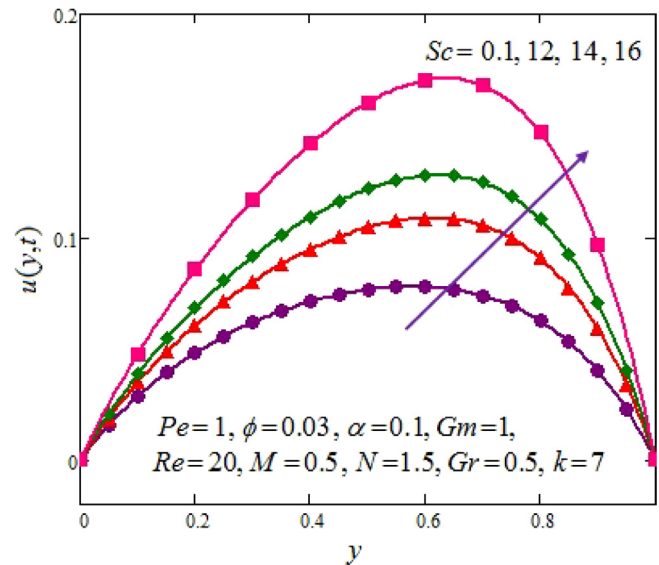


Fig. 15. Velocity profile for different values of Schmidt number  $Sc$ .

of nanofluid under change in physical process. Thermophysical properties of base fluid and nanoparticles are given in Table 1. The effect of different parameters on the flow, temperature and concentration of the fractional nanofluid  $\alpha \in (0,1)$ , and ordinary nanofluid ( $\alpha = 1$ ) is observed through Figs. 1–17.

Fig. 1 shows the effect of fractional parameter on fluid temperature. Temperature of nanofluid is a decreasing function of fractional parameter  $\alpha$ . The ordinary nanofluids have less temperature than those of fractional nanofluids. In Figs. 2 and 3, temperature is an increasing function of volume fraction  $\phi$  for both fractional and ordinary nanofluid while taking all other parameters constant. Physically, by increasing the volume fraction of nanoparticles to the base fluid enhance its thermal conductivity which makes the fluid hot. Fig. 4 shows that temperature of the nanofluid increases with the Radiation parameter  $N$  due to an increase in heat energy transfer to the fluid. Temperature of nanofluid is a decreasing function of Peclet number for fractional nanofluid shown in Fig. 5.

Figs. 6 and 7 shows concentration profile. It is depicted that Concentration of the nanofluid is shown to be decreasing with increasing values of Schmidt number and fractional parameter  $\alpha$ . Concentration

decreases for both ordinary and fractional nanofluid. Fig. 8 elaborates the impact of fractional parameter  $\alpha$  on fluid flow. It is obvious from the graph that velocity of the fluid decreases with increasing the fractional parameter  $\alpha$ . The fractional nanofluids have greater flow than the ordinary nanofluid ( $\alpha = 1$ ). The influence of Solutal Grashof number on fluid flow is shown in Fig. 9, velocity increases with elevation in values of  $Gm$ . The increasing values of  $Gm$  leads to augment the velocity of both fractional and ordinary nanofluid. An increase in  $Gm$  enhances concentration gradient which increases buoyancy forces. Thus, the fluid flow increases. In mass transfer, buoyancy forces are dependent on concentration gradient rather than temperature gradient. Fig. 10, illustrates the impact of  $Gr$  on fluid flow. We can see that fluid velocity increases with increase in  $Gr$ . Grashof number is the ratio of buoyancy and viscous force. An increase in  $Gr$  enhances temperature gradient which increases buoyancy forces and fluid flow rises. Fig. 11 shows the influence of permeability parameter  $k$  on velocity of fractional nanofluid. It is since increasing reduces friction of the nanofluid with channel wall hence increases the flow. Fig. 12 depicted influence of magnetic parameter  $M$  on the velocity profile. Flow of fractional nanofluid decreases with increasing  $M$ . It is due to the Lorentz forces

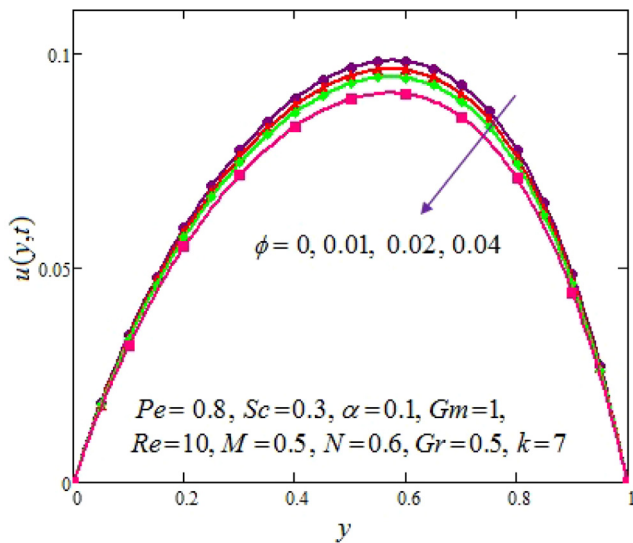


Fig. 16. Velocity profile for different values of Volume fraction  $\phi$ .

which reduces the flow. The Lorentz forces are maximum near the channel walls and minimum in the middle. Thus, velocity is minimum (Zero) at the boundaries and maximum in the center of the channel. Fig. 13 illustrates the effect of  $N$  on velocity profile. Increase in values of  $N$  increases amount of heat transfer to the fluid which increases the temperature of the fluid and in turn the flow of fractional nanofluid enhances. The velocity profile is a decreasing function of Peclet number  $N$  as shown in Fig. 14. The fluid flow is minimum at the boundaries and maximum in the middle. Fig. 15 shows that velocity of the fractional nanofluid increases with increasing Schmidt number  $Sc$ . Fig. 16 shows the impact of nanoparticles  $\phi$  on the flow of fractional nanofluid. The velocity of nanofluid slows down with increase in  $\phi$ . By adding more amounts of nanoparticles  $\phi$  to the fluid makes it more viscous which reduces their flow. Fig. 17 (a) and (b) shows the Nusselt number evolution with time  $t$  by varying the fractional parameter  $\alpha$ . The heat transfer rate is increasing at plate  $y = 0$ , but after some time while leading towards the plate  $y = 1$  it becomes constant. It is observed that for a smaller fractional parameter the rate of heat transfer is higher, it increases with decreasing values of  $\alpha$ . It means fractional nanofluids have high rate of heat transfer than ordinary nanofluid  $\alpha = 1$ . For Nusselt number at the other wall,  $y = 1$  is shown in Fig. 17 (b). A numerical estimation is made in Table 2 for Nusselt numbers  $Nu_1$  and  $Nu_2$

Table 2

Heat transfer rate variation with different values of fractional parameter and volume fraction.

Fractional parameter $\alpha$	$\phi = 0$	$\phi = 0.01$	$\phi = 0.02$	$\phi = 0.04$
<i>Nusselt number <math>Nu_1</math></i>				
0.01	1.128	1.162	1.196	1.265
0.2	1.154	1.188	1.222	1.291
0.4	1.184	1.217	1.251	1.322
0.6	1.211	1.245	1.279	1.35
1	1.217	1.249	1.283	1.351
<i>Nusselt number <math>Nu_2</math></i>				
0.01	0.753	0.777	0.802	0.853
0.2	0.704	0.728	0.753	0.805
0.4	0.645	0.669	0.694	0.745
0.6	0.573	0.579	0.621	0.671
1	0.573	0.579	0.621	0.671

of fractional nanofluid  $\alpha \in (0,1)$  and ordinary nanofluid ( $\alpha = 1$ ) for different values of  $\alpha$  and volume fraction of graphene nanoparticles. It is detected that the rate of heat transfer  $Nu_1$  and  $Nu_2$  enhances with increasing the volume fraction of nanoparticles. The thermal conductivity of the nanofluid increases by adding more amounts of graphene nanoparticles which enhances heat transfer rate. By coming down the rows in the Table 2 with the increasing values of  $\alpha$  heat transfer rate decreases and fractional nanofluid have higher rate of heat transfer than that of ordinary nanofluid. Fig. 18 (a) and (b) shows the skin friction at the two walls of the channel  $y = 0$  and  $y = 1$ . At wall  $y = 0$  shear stress decreases with increasing fractional parameter but after some time at  $t = 0.5$ , it takes a turn and shows an opposite behavior, here the graph starts increasing with increasing values of  $\alpha$  and the ordinary nanofluids curve is higher as compared to the fractional nanofluids' skin friction. At wall  $y = 0$  the skin friction increases with increasing fractional parameter and the ordinary nanofluid have the highest skin friction. At wall  $y = 1$  the skin friction is decreasing with fractional parameters. The same behavior is observed in numerical values in Table 3. Table 3 shows the numerical values of skin friction ( $Cf_1, Cf_2$ ) variation with  $\alpha$  and  $\phi$ . It's obvious that skin frictions  $Cf_1$  of the nanofluid increases by increasing the values of  $\phi$  and  $\alpha$ . From the table we observed that fractional nanofluid have less shear stress  $Cf_1$  than that of ordinary nanofluid. While  $Cf_2$  decreases with increase in  $\alpha$ . The fractional nanofluids have higher skin friction than ordinary nanofluid. For each value of  $\phi$  fractional nanofluids have less shear stress compared to ordinary nanofluid identical to Table 3. Numerical evaluation for Sherwood's number is shown in Table 4 for ( $Sh_1, Sh_2$ ). It is obvious

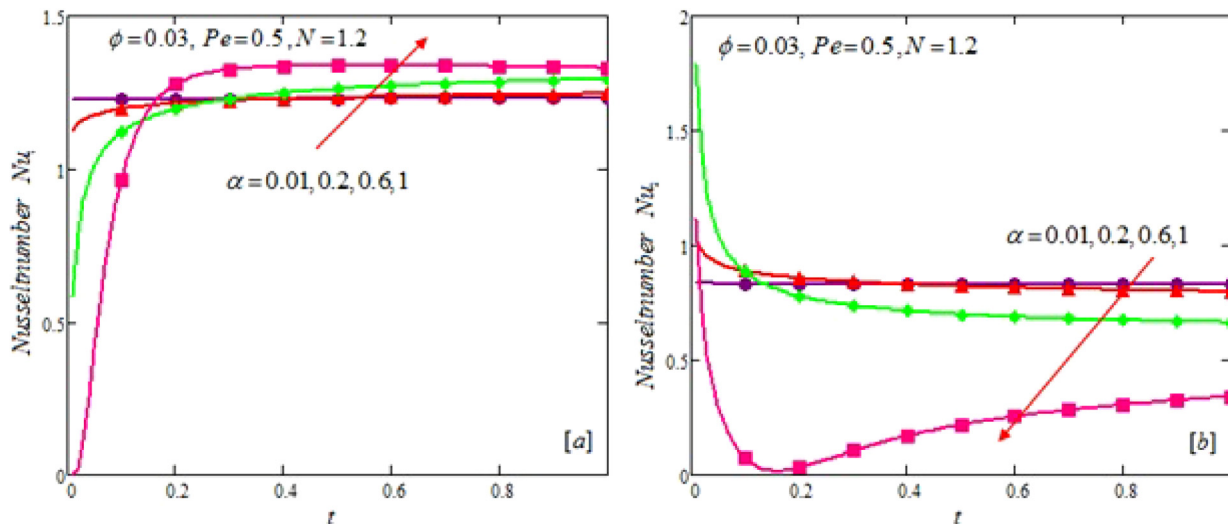


Fig. 17. Nusselt number variation for different values of Volume fraction  $\alpha$ .

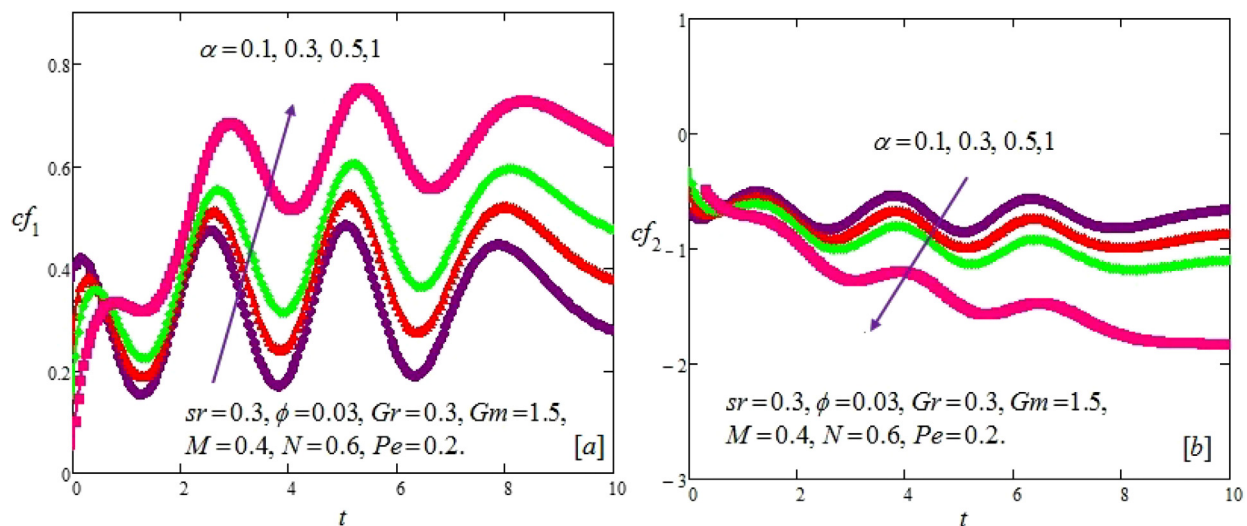


Fig. 18. Skin friction variation for different values of volume fraction  $\alpha$ .

**Table 3**  
Skin friction variation with different values of fractional parameter and volume fraction.

Fractional parameter $\alpha$	$\phi = 0$	$\phi = 0.01$	$\phi = 0.02$	$\phi = 0.04$
<i>Skin friction <math>Cf_1</math></i>				
0.1	0.448	0.499	0.45	0.453
0.3	0.466	0.467	0.468	0.47
0.6	0.494	0.495	0.469	0.497
1	0.552	0.552	0.552	0.552
<i>Skin friction <math>Cf_2</math></i>				
0.1	3.652	3.59	3.528	3.402
0.3	1.386	1.418	1.448	1.502
0.6	-379.838	-358.714	-338.235	-299.333
1	-334600	-310200	-286900	-243900

**Table 4**  
Variation of Sherwood's number with different values of fractional parameter and volume fraction.

Fractional parameter $\alpha$	$\phi = 0$	$\phi = 0.01$	$\phi = 0.02$	$\phi = 0.04$
<i>Sherwood's number <math>Sh_1</math></i>				
0.1	0.618	0.615	0.613	0.607
0.3	0.589	0.586	0.582	0.576
0.6	0.531	0.527	0.523	0.515
1	0.293	0.287	0.281	0.269
<i>Sherwood's number <math>Sh_2</math></i>				
0.1	1.88	1.887	1.895	1.911
0.3	1.907	1.914	1.923	1.939
0.6	1.744	1.752	1.76	1.776
1	0.52	0.523	0.525	0.531

that  $Sh_1$  decreases with increase in  $\phi$  and  $\alpha$ .  $Sh_2$  increases with

**Appendix A**

$$F(a, q, b, c) = \frac{\sinh[a\sqrt{q+b}]}{q\sinh[c\sqrt{q+b}]} = \sum_{n=0}^{\infty} \left[ \frac{1}{q} e^{-(2n+1)c-a}\sqrt{q+b} - \frac{1}{q} e^{-(2n+1)c+a}\sqrt{q+b} \right] \tag{A1}$$

$$f(a, t, b, c) = L^{-1}\{F(a, q, b, c)\} = \sum_{n=0}^{\infty} [\psi_n(a, t, b, c) - \psi_n(-a, t, b, c)]; \text{ where}$$

$$\psi_n(a, t, b, c) = \frac{1}{2} \left[ e^{-(2n+1)c-a}\sqrt{b} \operatorname{erfc} \left( \frac{(2n+1)c-a}{2\sqrt{t}} - \sqrt{bt} \right) + e^{(2n+1)c-a}\sqrt{b} \operatorname{erfc} \left( \frac{(2n+1)c-a}{2\sqrt{t}} + \sqrt{bt} \right) \right]$$

increasing volume fraction  $\phi$  and decreases with increasing  $\alpha$ . Fractional nanofluids have higher Sherwood's number as compared to ordinary nanofluids.

**Conclusions**

In this attempt, the exact solutions for unsteady MHD mixed convection problem of Maxwell fractional nanofluid are obtained using Caputo-time fractional derivatives. Expressions of velocity, concentration and temperature are acquired using Laplace transform method and then presented graphically for various embedded parameters. Some important outcomes are:

- Velocity increases with increase in  $Gr, Gm, Sc, N$  and  $k$  at time  $t$ .
- Velocity decreases with increasing values of  $M, Pe, \phi$  and  $\alpha$ .
- Velocity of fractional nanofluid is greater than that of ordinary nanofluid.
- Fractional nanofluid have higher rate of heat transfer and Sherwood's number than that of ordinary nanofluid.

$$H(a, q, b, c) = \frac{\sinh[a\sqrt{q^\alpha + b}]}{q^\alpha \sinh[c\sqrt{q^\alpha + b}]} = F(a, q^\alpha, b, c)$$

$$h(a, t, b, c) = L^{-1}\{H(a, q, b, c)\} = \begin{cases} \int_0^\infty t^{-1} f(a, x, b, c) \phi(0, -\alpha, -xt^{-\alpha}) dx; & 0 < \alpha < 1, \\ f(a, t, b, c), & \alpha = 1 \end{cases}; \quad (\text{A2})$$

where  $\phi(\beta, -\sigma, z) = \sum_{n=0}^{\infty} \frac{z^n}{n! \Gamma(\beta, -n\sigma)}$  is the Wright function

## References

- [1] Makinde OD, Mhone PY. Heat transfer to MHD oscillatory flow in a channel filled with porous medium. *Rom J Phys* 2005;931(50):9–10.
- [2] Al-Salem K, Öztop HF, Pop I, Varol Y. Effects of moving lid direction on MHD mixed convection in a linearly heated cavity. *Int J Heat Mass Transf* 2012;55(4):1103–12.
- [3] Salleh MZ, Nazar R, Pop I. Mixed convection boundary layer flow about a solid sphere with Newtonian heating. *Arch Mech* 2010;62(4):283–303.
- [4] Aaiza G, Khan I, Shafie S. Energy transfer in mixed convection MHD flow of nanofluid containing different shapes of nanoparticles in a channel filled with saturated porous medium. *Nanoscale Res Lett* 2015;10(1):490.
- [5] Salleh MZ, Nazar R, Pop I. Mixed convection boundary layer flow over a horizontal circular cylinder with Newtonian heating. *Heat Mass Transfer* 2010;46(11–12):1411–8.
- [6] Aman S, Khan I, Ismail Z, Salleh MZ. Impacts of gold nanoparticles on MHD mixed convection Poiseuille flow of nanofluid passing through a porous medium in the presence of thermal radiation, thermal diffusion and chemical reaction. *Neural Comput Appl* 2016;1–9.
- [7] Aman S, Khan I, Ismail Z, Salleh MZ, Alshomrani AS, Alghamdi MS. Magnetic field effect on Poiseuille flow and heat transfer of carbon nanotubes along a vertical channel filled with Casson fluid. *AIP Adv* 2017;7(1):015036.
- [8] Mujeebu MA, Abdullah MZ, Bakar MA, Mohamad AA, Abdullah MK. Applications of porous media combustion technology—a review. *Appl Energy* 2009;86(9):1365–75.
- [9] Maxwell JC. A treatise on electricity and magnetism. Dover Publications; 1873.
- [10] Choi SU, Jeffrey A, Eastman. Enhancing thermal conductivity of fluids with nanoparticles. No. ANL/MSD/CP-84938; CONF-951135–29. Argonne National Lab., IL (United States); 1995.
- [11] Vincenzo B, Manca O, Nardini S, Vafai K, editors. Heat transfer enhancement with nanofluids. first ed. CRC Press; 2015.
- [12] Turkyilmazoglu M, Pop I. Heat and mass transfer of unsteady natural convection flow of some nanofluids past a vertical infinite flat plate with radiation effect. *Int J Heat Mass Transf* 2013;59:167–71.
- [13] Hayat T, Asad S, Alsaedi A. Flow of Casson fluid with nanoparticles. *Appl Math Mech* 2016;37(4).
- [14] Sheikholeslami M, Ellahi R. Electrohydrodynamic nanofluid hydrothermal treatment in an enclosure with sinusoidal upper wall. *Appl Sci* 2015;5(3):294–306.
- [15] Sheikholeslami M, Zia QM, Ellahi R. Influence of induced magnetic field on free convection of nanofluid considering Koo-Kleinstreuer-Li (KKL) correlation. *Appl Sci* 2016;6(11):324.
- [16] Hussanan A, Khan I, Hashim H, Mohamed MKA, Ishak N, Sarif NM, Salleh MZ. Unsteady MHD flow of some nanofluids past an accelerated vertical plate embedded in a porous medium. *J Teknologi* 2016;78(2).
- [17] Hussanan A, Salleh MZ, Khan I, Shafie S. Convection heat transfer in micropolar nanofluids with oxide nanoparticles in water, kerosene and engine oil. *J Mol Liq* 2017;229:482–8.
- [18] Prabhakar B, Bandari S, Haq RU. Impact of inclined Lorentz forces on tangent hyperbolic nanofluid flow with zero normal flux of nanoparticles at the stretching sheet. *Neural Comput Appl* 2016;1–10.
- [19] Halelfadl S, Maré T, Estellé P. Efficiency of carbon nanotubes water based nanofluids as coolants. *Exp Therm Fluid Sci* 2014;53:104–10.
- [20] Magyari E. Comment on the homogeneous nanofluid models applied to convective heat transfer problems. *Acta Mechanica* 2011;222(3):381–5.
- [21] Khan I. Shape effects of MoS<sub>2</sub> nanoparticles on MHD slip flow of molybdenum disulphide nanofluid in a porous medium. *J Mol Liq* 2017;233:442–51.
- [22] Tyagi H, Patrick P, Prasher R. Predicted efficiency of a low-temperature nanofluid-based direct absorption solar collector. *J Solar Energy Eng* 2009;131(4):041004.
- [23] Yousefi T, Veysi F, Shojaeizadeh E, Zinadini S. An experimental investigation on the effect of Al<sub>2</sub>O<sub>3</sub>-H<sub>2</sub>O nanofluid on the efficiency of flat-plate solar collectors. *Renewable Energy* 2012;39(1):293–8.
- [24] Zamani H, Mahian O, Rashidi I, Lorenzini G, Wongwises S. Exergy optimization of a double-exposure solar cooker by response surface method. *J Therm Sci Eng Appl* 2017;9(1):011003.
- [25] Mahian O, Kianifar A, Heris SZ, Wen D, Sahin AZ, Wongwises S. Nanofluids effects on the evaporation rate in a solar still equipped with a heat exchanger. *Nano Energy* 2017;36:134–55.
- [26] Mahian O, Kianifar A, Heris SZ, Wongwises S. Natural convection of silica nanofluids in square and triangular enclosures: theoretical and experimental study. *Int J Heat Mass Transf* 2016;99:792–804.
- [27] Vieru D, Fetecau C, Fetecau C. Time-fractional free convection flow near a vertical plate with Newtonian heating and mass diffusion. *Therm Sci* 2015;19(1):85–98.
- [28] Kulish VV, Lage JL. Application of fractional calculus to fluid mechanics. *J Fluids Eng* 2002;124(3):803–6.
- [29] Ali F, Saqib M, Khan I, Sheikh NA. Application of Caputo-Fabrizio derivatives to MHD free convection flow of generalized Walters'-B fluid model. *Eur Phys J Plus* 2016;131(10):377.
- [30] Azhar WA, Vieru D, Fetecau C. Free convection flow of some fractional nanofluids over a moving vertical plate with uniform heat flux and heat source. *Phys Fluids* 2017;29(8):082001.
- [31] Imran MA, Raza N, Abdullah M, Aleem M. Wall slip and non-integer order derivative effects on the heat transfer flow of Maxwell fluid over an oscillating vertical plate with new definition of fractional Caputo-Fabrizio derivatives. *Results Phys* 2017.
- [32] Cao Z, Zhao J, Wang Z, Liu F, Zheng L. MHD flow and heat transfer of fractional Maxwell viscoelastic nanofluid over a moving plate. *J Mol Liq* 2016;222:1121–7.
- [33] Fetecau C, Vieru D, Azhar WA. Natural convection flow of fractional nanofluids over an isothermal vertical plate with thermal radiation. *Appl Sci* 2017;7(3):247.
- [34] Pan M, Zheng L, Liu F, Liu C, Chen X. A spatial-fractional thermal transport model for nanofluid in porous media. *Appl Math Model* 2018;53:622–34.
- [35] Abro KA, Hussain M, Baig MM. An analytic study of molybdenum disulfide nanofluids using the modern approach of Atangana-Baleanu fractional derivatives. *Eur Phys J Plus* 2017;132(10):439.
- [36] Cao Z, Zhao J, Zheng L. Fractional boundary-layer Flow and heat transfer of a Nanofluid over an unsteady moving plate. *Heat Transfer Research*. 2017;48(17).
- [37] Cogley AC, Gilles SE, Vincenti WG. Differential approximation for radiative transfer in a nongrey gas near equilibrium. *AIAA J* 1968;6(3):551–3.